JACS
JOURNAL OF THE AMERICAN CHEMICAL SOCIETY

Article

pubs.acs.org/JACS

Reduction of α,β-Unsaturated Ketones by Old Yellow Enzymes: Mechanistic Insights from Quantum Mechanics/Molecular Mechanics Calculations

Richard Lonsdale[†,‡] and Manfred T. Reetz*[,†,‡]

[†]Max-Planck-Institut für Kohlenforschung, Kaiser-Wilhelm-Platz 1, 45470 Mülheim an der Ruhr, Germany

[‡]Fachbereich Chemie der Philipps-Universität, Hans-Meerwein-Strasse, 35032 Marburg, Germany

Supporting Information

ABSTRACT: Enoate reductases catalyze the reduction of activated C═C bonds with high enantioselectivity. The oxidative half-reaction, which involves the addition of a hydride and a proton to opposite faces of the C═C bond, has been studied for the first time by hybrid quantum mechanics/molecular mechanics (QM/MM). The reduction of 2-cyclohexen-1-one by YqjM from *Bacillus subtilis* was selected as the model system. Two-dimensional QM/MM (B3LYP-D/OPLS2005) reaction pathways suggest that the hydride and proton are added as distinct steps, with the former step preceding the latter. Furthermore, we present interesting insights into the reactivity of this enzyme, including the weak binding of the substrate in the active site, the role of the two active site histidine residues for polarization of the substrate C═O bond, structural details of the transition states to hydride and proton transfer, and the role of Tyr196 as proton donor. The information presented here will be useful for the future design of enantioselective YqjM mutants for other substrates.

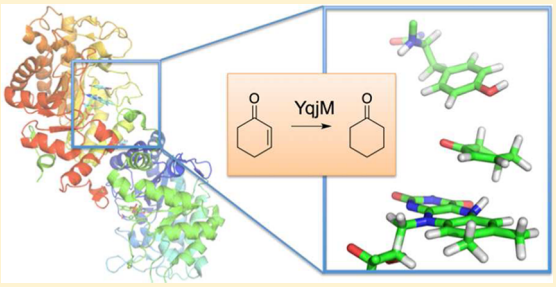

INTRODUCTION

The enantioselective conjugate reduction of prochiral α,β-unsaturated ketones is of considerable interest in the field of organic synthesis, representing one of the major routes for the generation of chiral molecules. Due to ecological and economical reasons, catalytic processes are preferred, chiral transition-metal complexes,[1] organocatalysts,[2] or enzymes.[3] When opting for biocatalysis, the old yellow family of enzymes (OYEs), which are NADPH-dependent flavin oxidoreductases, are used most often.[3,4] OYEs can be engineered to modify selectivity, however, a more detailed picture of the mechanism may help in the design of more reactive/selective mutants.

YqjM is an OYE family member that is involved in the oxidative stress defense mechanism in *Bacillus subtilis*.[5,6] YqjM, as with other OYEs, has also been found to catalyze the reduction of the C═C double bonds of α,β-unsaturated ketones, as exemplified by the reaction of 2-cyclohexen-1-one (**1**) (Scheme 1). For substrates with substituents on the double bond, reduction often occurs in a stereospecific manner.[7] In those cases in which stereoselectivity is poor, protein engineering has been applied.[8−12]

Scheme 1. Reduction of 2-Cyclohexen-1-one (1) to Cyclohexanone (2) Catalyzed by YqjM

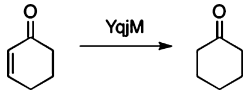

OYEs operate via a "ping-pong" mechanism made up of two half-reactions. During the reductive half-reaction NADPH binds in the active site and reduces the flavin cofactor from FMN to $FMNH^-$. The reduction of FMN by NADPH has been suggested to occur via hydrogen tunneling in the OYE morphinone reductase (MR).[13,14] $NADP^+$ is subsequently replaced in the active site by the substrate, which then undergoes C═C reduction by the $FMNH^-$, resulting in formation of the product and oxidized flavin, FMN (hence termed the oxidative half-reaction).

The proposed mechanism for the oxidative half-reaction in OYEs involves two steps (Scheme 2): (1) hydride transfer from N5 of the flavin mononucleotide; (2) proton transfer from solvent via Tyr169. It has been suggested that the hydride and proton may be transferred to the substrate simultaneously.[13] The details for the proton transfer step have not been conclusively determined. It is not known whether the proton comes directly from Tyr169 or whether a water molecule held in position by the Tyr169 donates the proton. Mutation of the corresponding residue in OYE1 to phenylalanine resulted in a dramatic (but not complete) loss of activity in the oxidative half-reaction, but had no effect on the reductive half-reaction.[15] This suggests that water, or some other proton donor, may be used in the absence of Tyr169.

Received: August 17, 2015
Published: October 31, 2015

DOI: 10.1021/jacs.5b08687
J. Am. Chem. Soc. 2015, 137, 14733−14742

Scheme 2. Proposed Mechanism[a] for the Reduction of Substrate 1 by YqjM[13−16]

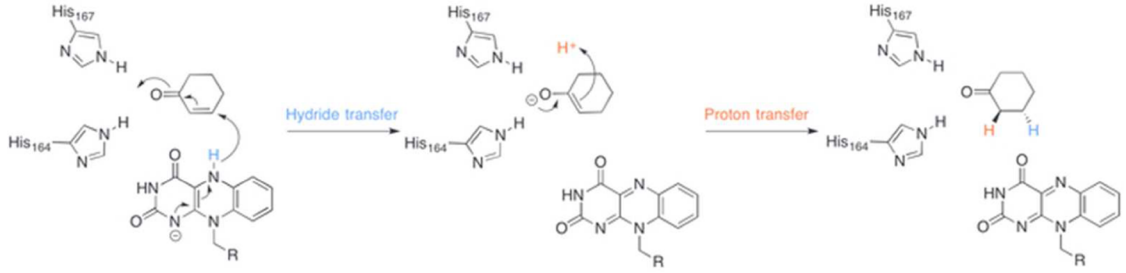

[a]The hydride (blue) and proton (red) are added across the C═C bond in a *trans* fashion.

The stereochemistry of product formation is widely accepted to be determined by the orientation of the substrate in the active site. The hydride and proton are added in a trans fashion. In the case of substrates substituted at the position β- to the electron-withdrawing group (EWG), the substrate can bind in two orientations in which the EWG forms hydrogen bonds to the two active site histidines. In other OYEs, one or both of the histidines are replaced by asparagine. The first orientation places the olefinic double bond of the substrate directly above the flavin, and the other orientation places the C−C bond opposite to this position above the flavin. These two orientations are referred to herein as "normal" and "flipped", respectively.[16] In the case of the model substrate here, with no substituent β- to the carbonyl, the same product will be formed, regardless of the face of the double bond that the hydride approaches from.

X-ray crystal structures of YqjM revealed several structural features that are unique to this enzyme compared to the other known OYEs.[17] YqjM shares the same overall fold as the rest of the OYE family, however, unlike the rest of the family which functions as monomers or dimers, YqjM functions as a homotetramer. In OYE1, a threonine residue regulates the redox potential of the flavin.[18] This residue is replaced with a cysteine in YqjM. Additionally, the C-terminal region of the neighboring subunit is found to directly interact with the substrate in the active site of Yqjm, a feature not observed in other OYE enzymes.

While some details of the catalytic mechanism of reduction by OYEs are known from experimental studies,[13−18] some details are not entirely understood. Theoretical studies, such as those employing hybrid quantum mechanics/molecular mechanics (QM/MM), can provide important insight into mechanistic details that may not be possible via experimental means.[19−24] Relatively few theoretical studies have been performed on the OYE family. A theoretical study was performed on OYE1 by Chateauneuf et al., who investigated the charge-transfer interactions between the FMN cofactor and a phenolate anion using the semiempirical ZINDO/S method.[25] The reductive half-reaction in morphinone reductase has been studied using QM/MM by Pang et al., where the contribution of tunneling was investigated using variational transition-state theory.[14] The authors estimated that 99% of the hydride transfer from NADH to the flavin occurs via tunneling, despite the experimentally observed kinetic isotope effect being below the semiclassical limit. Although not a member of the OYE family, the protochlorophyllide oxidoreductase enzyme catalyzes the *trans*-addition of hydrogen across a C═C bond. Heyes et al. unveiled a sequential hydride and proton transfer mechanism to this enzyme by applying DFT methods.[26]

In the current study, we use QM/MM calculations to shed light on the mechanistic details of the reduction of 2-cyclohexen-1-one (**1**) by YqjM. **1** is frequently used as a model substrate for studying OYEs and hence provides us with experimental data with which to validate our findings. We address details such as those concerning the binding of the substrate to the active site, the order of the reaction steps, and the nature of the transition states to hydride and proton transfer. Additionally, we investigate the roles of the active site residues in the catalyzed reaction and explore the likely proton source.

METHODS AND COMPUTATIONAL DETAILS

Protein Model. The crystal structure of YqjM in complex with *p*-nitrophenol (PDB entry 1Z44)[17] was used as the basis for this study. The protein was prepared for simulation using the Protein Preparation Wizard in the Maestro program.[27] The 1Z44 crystal structure is a homodimer, where part of the B-chain interacts with the active site of the A-chain and vice versa. Hence, both chains were retained in all of the calculations presented here. Protonation states for titratable amino acids were assigned based on the most favorable interactions with neighboring residues and the PROPKA program.[28] The His164 and His167 residues, which are believed to be important in the binding of the substrate in the active site, were protonated at the epsilon and delta nitrogen atoms, respectively. In these protonation states, the N−H side chain groups were oriented such that interaction with the substrate could occur. All water molecules and co-crystallized ligands were removed, with the exception of the FMN cofactors.

Ligand Preparation. Substrate **1** was built in Maestro and prepared for docking using the LigPrep program.[29]

Docking. Substrate **1** was docked into the active site of YqjM using the induced fit docking (IFD) protocol within the Schrödinger suite.[30−33] Further details are provided in the Supporting Information (SI).

Molecular Dynamics Simulations. Molecular dynamics (MD) simulations were performed using the Desmond program.[34−37] The OPLS-2005 all-atom MM force field was used.[38] Simulations were performed using periodic boundary conditions. The protein was solvated in an orthorhombic box of TIP3P water molecules[39] with a buffer of at least 10 Å surrounding the protein. The charge of each model was neutralized by the addition of sodium ions. A time step of 2.0 fs was used throughout the simulations, which were performed at constant temperature (300 K) and pressure (1.01325 bar). The Nose−Hoover thermostat and Martyna−Tobias−Klein barostat were used, with relaxation times of 1.0 and 2.0 ps, respectively. The particle mesh Ewald method was used for the treatment of long-range interactions, and a nonbonded cutoff of 9.0 Å was used for short-range interactions. A random seed was used in the generation of the initial velocities. Simulations were each run for 20 ns.

QM/MM Calculations. Starting geometries for the QM/MM calculations were obtained at random from the MD simulations detailed above. Each system was truncated by the removal of water and sodium ions such that the protein was surrounded by a 5 Å layer of

DOI: 10.1021/jacs.5b08687
J. Am. Chem. Soc. 2015, 137, 14733−14742

solvent. All atoms in the truncated system were energy-minimized at the MM level using conjugate gradient (energy convergence = 10^{-7} kcal/mol), followed by truncated Newton (100 steps) minimization within the Impact program.[40] QM/MM calculations were performed using the QSite program.[41−43] The QM region consisted of the substrate, the flavin mononucleotide truncated at the C1 position, and the side-chain atoms of Y169 (see Figure 1). Additionally, the water molecule located between the substrate and Y169 was included in the QM region when considering water as a proton donor. QM calculations were performed at the unrestricted-B3LYP/6-31G(d) level of theory. Each QM model system had an overall charge of −1. The rest of the system was treated MM with the OPLS-2005 force field. Where the QM-MM partition was across a covalent bond, a frozen-orbital approach was used, with a Gaussian charge distribution used to represent the MM charges in the vicinity of the QM-MM boundary. Reactions were modeled by constructing energy profiles mapping the QM/MM energy against an appropriately selected reaction coordinate, as depicted in Figure 1. The reaction coordinate was varied at 0.2 Å intervals. MM atoms that were at a distance >5 Å to the QM region were held fixed. Transition states were optimized using the quadratic synchronous transit method. Single point energies were performed on the optimized geometries of all stationary points on the minimum energy pathways at the B3LYP/cc-pVTZ(-f) level. Two-dimensional (2D) potential energy surfaces were computed by varying the two reaction coordinates corresponding to hydride and proton transfer simultaneously. This was achieved by first computing a 1D surface for the hydride transfer pathway and then using each of the optimized structures as the starting point for proton transfer pathways with the hydride transfer coordinate held fixed. In a previous QM/MM study it was shown that inclusion of dispersion can be important for comparing the energy barriers for different reaction mechanisms.[44] For this reason, reported energy barriers include single point energy corrections using Grimme's D3 empirical formalism.[45]

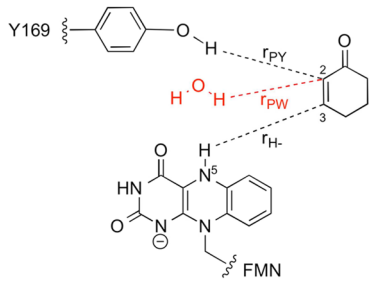

Figure 1. QM region used in QM/MM calculations. The wavy lines depict where the QM/MM boundary bisects a covalent bond. The atoms depicted in black were included in all QM/MM calculations, while the water molecule (red) was only included when considered as the proton donor. The dotted lines define the reaction coordinates used during reaction modeling: r_{H-} is the hydride transfer reaction coordinate; r_{PY} refers to direct proton transfer from Y169; r_{PW} refers to proton transfer from Y169 via a bridging water molecule.

QM Model Calculations. Single point energies were calculated on the QM regions of selected QM/MM-optimized geometries using Jaguar,[46,47] with the same DFT functional and basis set that was used for the QM/MM calculations. The standard Poisson−Boltzmann continuum solvation model (for water) was used.

RESULTS AND DISCUSSION

Docking. To investigate the binding of substrate **1** in the active site of YqjM, IFD calculations were performed. IFD allows flexibility of the residues surrounding the binding pocket, enabling a more favorable substrate binding position. A total of 19 binding poses were found (details in SI). The highest ranked docking pose places the substrate in the "normal" binding position, as expected (Figure 2a). The fourth-highest ranked docking pose corresponds to the flipped docking pose (Figure 2b) and has a binding energy that is 1.7 kcal/mol less favorable than the "normal" pose (calculated using IFDScore). The distance between the flavin N5-hydride and the substrate C3 atom is 3.59 and 3.77 Å in the normal and flipped poses, respectively. Hence from this docking study it appears that substrate **1** preferentially binds to the enzyme in the normal pose. In both docking poses the substrate oxygen forms hydrogen bonds to H164 and H167.

MD Simulations. To investigate the conformational stability of the substrate in the active site and to relax the simulation system for QM/MM calculations, MD simulations were performed. The docking poses described above and depicted in Figure 2 were used as starting structures (details are provided in the Methods and Computational Details section). In preliminary unrestrained MD simulations using both docking poses, the hydrogen bonds between the substrate and H164 and H167 were broken after <1 ns. Alternative protonation states of H164 and H167 were tested, but in all cases the hydrogen bonds between the substrate and these residues were not maintained, and the substrate moved from its position above the flavin. The active site is very close to the surface of the protein and is therefore exposed to the

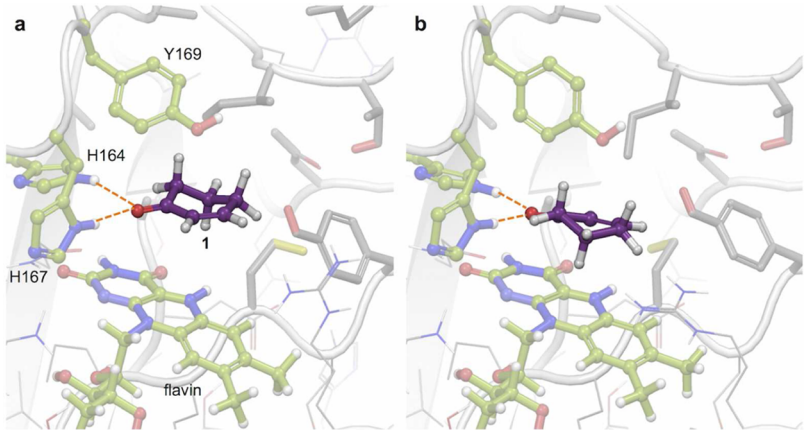

Figure 2. IFD of **1** in the active site of YqjM. (a) Highest ranked docking pose, corresponding to the "normal" orientation of the substrate in the active site. (b) Fourth-highest ranked docking pose, which places the substrate in the "flipped" binding orientation. Interactions between the substrate carbonyl oxygen and H164 and H167 are shown by orange dashed lines.

DOI: 10.1021/jacs.5b08687
J. Am. Chem. Soc. 2015, 137, 14733−14742

surrounding solvent. Previous experimental work has suggested that **1** does not bind very strongly to the active site of YqjM[s] and may explain the weak binding observed in our simulations. Substrate **1** is not a natural substrate for YqjM and does not possess a polar group that can interact with R337 of the B-chain, which may help to explain the poor binding in the active site. As one of the primary aims of the MD simulations is to generate different starting structures for QM/MM modeling, further simulations were run where the original protonation states of H167 and H164 were used, but in which harmonic restraints (10 kcal/mol Å^2) were placed between the oxygen atom of the substrate and the side chain N−H groups of H167 and H164, in order to keep them close to their original values.

During the simulations of substrate **1** in the "normal" and "flipped" orientations, the substrate remains in the same binding position for the entire simulation. The distances between the substrate C3 and C2 atoms with the flavin N5 hydride and Y169 proton, respectively, were monitored over the course of the simulations. The values of these distances fluctuated over average values of 3.61 and 4.83 Å (see SI Figure S1). The corresponding average distances for the simulation of substrate **1** in the "flipped" orientation were 3.89 and 3.98 Å (SI Figure S2). Hence the hydride is closer to the substrate in the "normal" pose, compared to the "flipped" pose, however, the opposite is true for the proton. A conformational change occurs during the simulation of the "flipped" binding pose after approximately 10 ns of simulation time, and the flavin moves closer to the substrate. The average distance between the C3 atom of the substrate and the flavin N5 hydride is 4.64 Å before the conformational change and 3.22 Å afterward. The conformational change coincides with a movement of R307, which maintains a salt bridge to the phosphate group of the flavin cofactor. For the whole simulation of the "flipped" binding pose and the majority of that of the "normal" pose, the OH group of Y169 points away from the substrate. In this orientation, the OH group interacts with nearby water molecules. However, a small proportion of the simulation time for the "normal" binding pose exhibited structures where the OH group of Y169 was pointing toward the C=C bond of the substrate. Structures from these restrained MD simulations were used as the starting point for QM/MM modeling, described in the QM/MM Calculations section.

QM/MM Calculations. *Substrate Binding.* A possible role of the hydrogen-bonding interactions from H167 and H164 is to lower the energy of the LUMO of the substrate, facilitating the transfer of hydride to the substrate. To investigate the effect of the enzyme environment on the LUMO of the substrate, the highest occupied and lowest unoccupied molecular orbitals (HOMO−LUMO) energy gap of **1** in solution was compared to that in the enzyme environment (for the "normal" substrate binding orientation). The HOMO−LUMO gap for the enzyme system was computed by first performing a QM/MM geometry optimization on a structure taken from the restrained MD simulation using the QM region shown in Figure 1, and a subsequent single point energy calculation was performed on this optimized geometry with only the substrate included in the QM region. For the model of the substrate in solution, all atoms were removed from the QM/MM optimized structure, with the exception of the substrate, and a single point energy calculation was performed using a continuum solvation model. The HOMO and LUMO of the substrate calculated in the enzyme and in solution are depicted in Figure 3, together with their respective energies. The HOMO−LUMO gaps of **1** in solution and in the enzyme are 5.32 and 5.34 eV, respectively. This shows that the inclusion of the enzyme environment using a point-charge model does not lower the energy of the LUMO of the substrate relative to the HOMO. Inspection of the HOMO and LUMO surfaces in Figure 3 reveals that the hydrogen bonds between H164 and H167 point into the HOMO of the substrate, rather than the LUMO, therefore it is unlikely that these residues will lower the energy of the LUMO relative to the HOMO, consistent with our calculated HOMO−LUMO energy gaps.

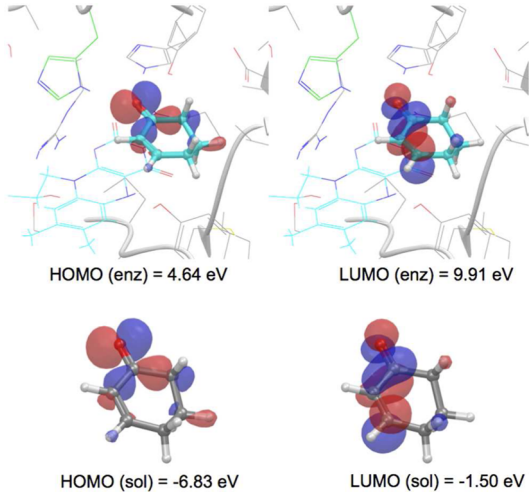

Figure 3. HOMO and LUMO of **1** in the active site of YqjM (enz) and vacuum with implicit solvent correction (sol). The enzyme-bound state corresponds to the "normal" binding pose.

A comparison of the calculated atomic charges of the substrate in the enzyme and solution reveals that the substrate C=O bond is significantly more polarized in the enzyme (see SI Table S2). To evaluate the contribution of H164 and H167 to the polarization effect of the substrate in the enzyme, a QM/MM single point energy calculation of the substrate (QM) was performed with only the H164 and H167 (MM) residues included. The calculated charges from the latter calculation are in close agreement with those corresponding to inclusion of the whole enzyme, indicating that H164 and H167 are responsible for the enhancement in the polarization of the substrate C=O bond. Increasing the polarization of the C=O bond in the substrate will facilitate the formation of the enolate intermediate following the hydride transfer step.

Reaction Mechanism. During the reduction of α,β-unsaturated ketones by the OYE family, a proton and hydride ion are added to the C=C moiety of the substrate, from opposite faces of the π-system. The hydride is supplied by the reduced flavin species, whereas there are two plausible pathways by which the proton can be supplied that are consistent with both the high stereospecificity observed for this enzyme and the dramatic loss of activity for the Y169F mutant in analogous members of the OYE family:[15] Direct proton transfer to C2 from Y169 or proton transfer from Y169 via a bridging water molecule. Both of these possibilities have been considered here.

As mentioned in the Introduction, it has not been conclusively determined whether the proton and hydride are added simultaneously or as distinct steps. In order to first determine the order of events, 2D potential energy surfaces were generated, with the hydride and proton transfer reaction

DOI: 10.1021/jacs.5b08687
J. Am. Chem. Soc. 2015, 137, 14733−14742

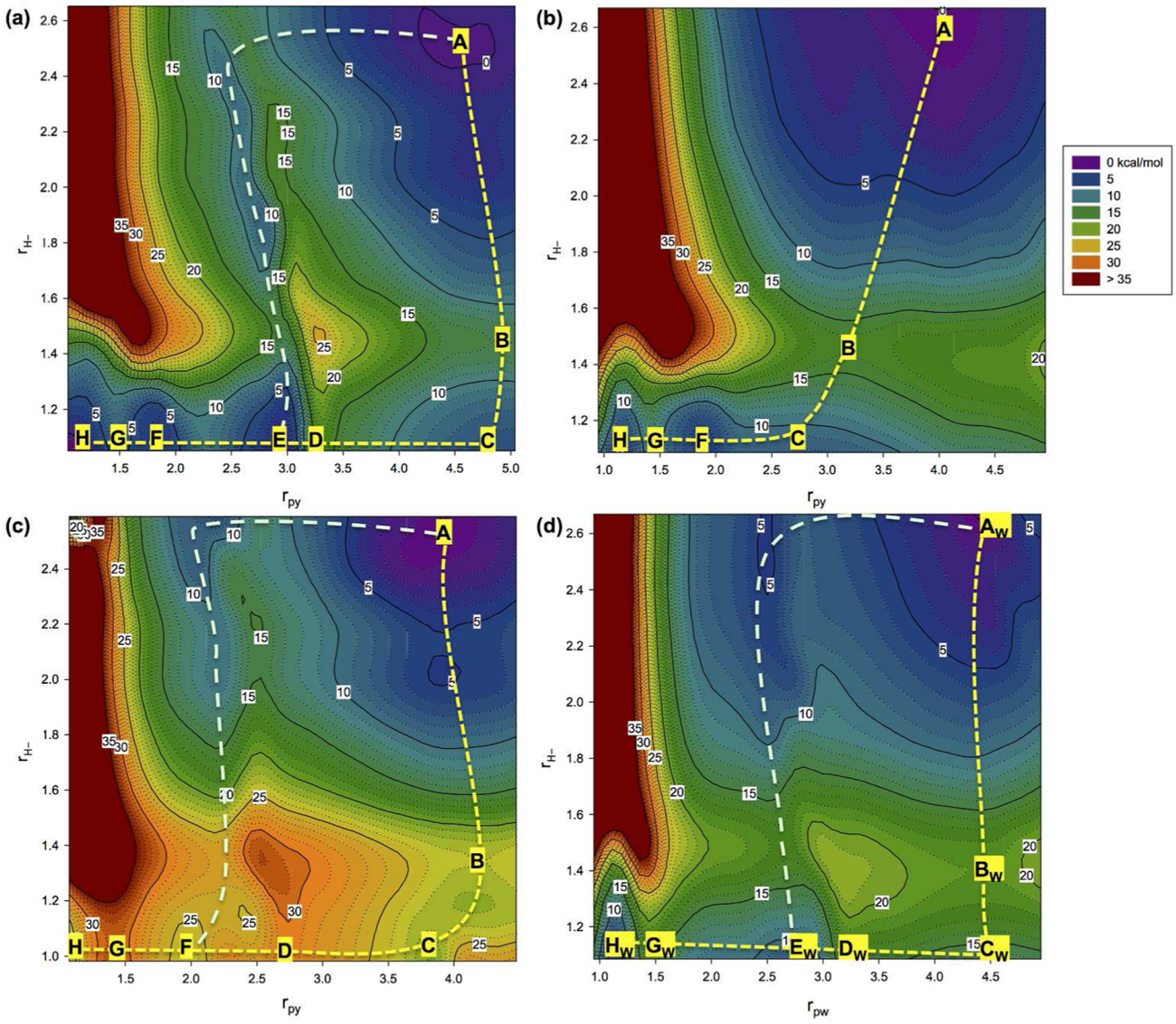

Figure 4. 2D potential energy surfaces for the reduction of substrate **1** by YqjM (calculated at the B3LYP-6-31G(d)/OPLS2005 level): (a) with substrate in normal orientation and Y169 as proton donor (O−H group of Y169 pointing away from substrate in initial structure); (b) substrate in normal orientation and Y169 as proton donor (O−H group of Y169 pointing toward substrate in initial structure); (c) substrate in flipped orientation and Y169 as proton donor (O−H group of Y169 pointing away from substrate in initial structure); and (d) substrate in normal orientation and Y169 acts as proton donor via bridging water molecule. The minimum energy pathways are displayed in yellow and green dashed lines. The stationary points **A**−**H** and $\mathbf{A_W}$−$\mathbf{H_W}$ are defined in Scheme 3. Energies are provided in kcal/mol relative to the reactant complex.

Scheme 3. Stationary Points Located on the 2D Potential Energy Surfaces for Reduction of Substrate 1 by YqjM Shown in Figure 4

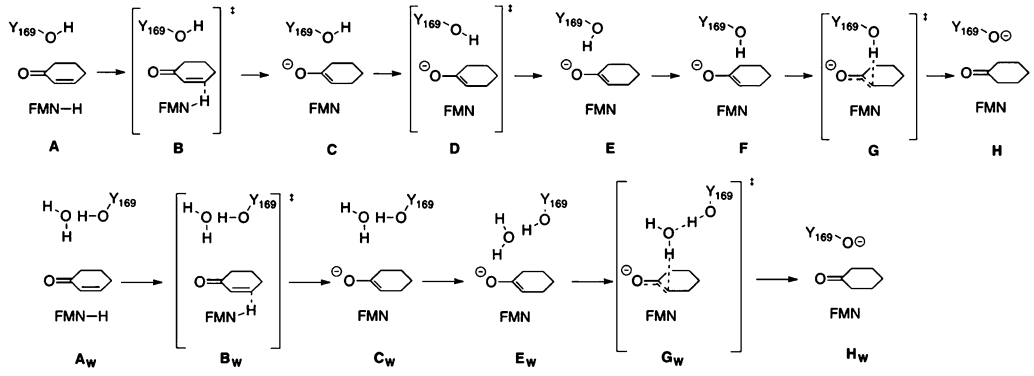

DOI: 10.1021/jacs.5b08687
J. Am. Chem. Soc. 2015, 137, 14733−14742

coordinates varied simultaneously. Starting structures were selected from the restrained MD simulations of the "normal" and "flipped" substrate binding orientations. For the "normal" substrate binding position, the Y169 hydroxyl group points away from the substrate for the majority of the MD simulation, however, for a small proportion of the time the hydroxyl group points toward the C═C bond of the substrate. For this reason, potential energy surfaces were computed for both conformations of Y169 (Figure 4a,b, respectively). There is insufficient space for a bridging water molecule to be located between the Y169 side chain and the substrate in the "flipped" conformation, hence only the direct proton transfer could be modeled for this conformation (Figure 4c). The protonation mechanism involving a bridging water molecule was modeled for the "normal" substrate binding pose (Figure 4d). The minimum energy pathway leading from reactant to product will indicate (1) whether the proton and hydride are added simultaneously and (2) if not, whether the proton or hydride is added first.

All of the lowest energy pathways across the 2D potential energy surfaces shown in Figure 4 suggest that it is energetically most favorable for the hydride and proton transfer steps to occur as separate steps, with the former occurring first. The hydride transfer from the N5 of the reduced flavin $FMNH^-$ to the substrate C3 atom results in the formation of an enolate intermediate, denoted **C** or $\mathbf{C_W}$ in Figure 4. The stationary points located on the minimum energy pathways in Figure 4 are described in Scheme 3, and the energies are displayed in Table 1.

Table 1. QM/MM Energies [in kcal/mol] of the Reaction Species A–H from the 2D Potential Energy Surfaces Shown in Figure 4[a]

species	(a)	(b)	(c)	(d)
A	0	0	0	0
B	14.2	16.4	22.2	19.0
C	8.3	9.2	20.4	14.7
D	17.4	–	28.4	17.2
E	3.6	–	36.4	9.2
F	7.1	7.7	28.0	10.2
G	10.2	16.3	34.2	17.2
H	2.1	11.3	34.7	9.5

[a]Calculated at the at the B3LYP-D3:cc-pVTZ(-f)/OPLS2005//B3LYP:6-31G(d)/OPLS2005 level.

In the case of the normal binding pose with the Y169 proton initially pointing away from the substrate (Figure 4a), there are two energetically feasible pathways leading from reactants to products. The first, indicated by a yellow dashed line in Figure 4a, involves hydride transfer from the reactant complex (**A**) to the enolate intermediate (**C**) via a transition state (**B**). This step has a barrier of 14.2 kcal/mol (calculated at the B3LYP-D3:cc-pVTZ(-f)/OPLS2005//B3LYP:6-31G(d)/OPLS2005 level). The energy of the enolate intermediate (**C**) is 8.3 kcal/mol relative to the reactant complex (**A**). The Y169 side chain OH group subsequently rotates to face the substrate, via a stationary point (**D**), with a barrier of 17.4 kcal/mol. This leads to intermediates (**E**) and (**F**), the latter undergoing proton transfer via a transition state (**G**) with a barrier of 10.2 kcal/mol to form the product complex (**H**). A second pathway is possible whereby (**A**) proceeds to (**E**) via initial rotation of Y169 followed by hydride transfer. This pathway is shown as a green dashed line in Figure 4a. It appears that the rotation of Y169 does not have an effect on the barrier to hydride transfer and can therefore occur either before or after this step. Hence, the rate-limiting step for this pathway is the hydride transfer step, and the overall energy barrier amounts to 17.4 kcal/mol.

In the case of the normal binding pose with the Y169 proton pointing toward the substrate in the initial step (Figure 4b), the reaction proceeds via hydride transfer (**B**) with a barrier of 16.4 kcal/mol. The enolate intermediate (**C**) is 9.2 kcal/mol higher in energy than the reactant complex (**A**) and undergoes subsequent proton transfer from Y169 (**G**) with an energy barrier of 16.3 kcal/mol. The orientation of Y169 hence has little effect on the overall barrier to reaction, as the reaction energetics for Figure 4a,b are similar (within ∼1 kcal/mol).

For the potential energy surface calculated for the flipped binding pose of substrate **1** (Figure 4c), the overall shape of surface is similar to that of the analogous pathway for the normal binding pose (Figure 4a). However, in the case of the flipped binding pose, the energy barriers are considerably higher. The energy barrier to hydride transfer (**B**) is 22.2 kcal/mol. The rotation of the Y169 hydroxyl group (**D**) has a barrier of 28.4 kcal/mol. The proton transfer step (**G**) has an energy barrier of 34.2 kcal/mol and is hence the rate-limiting step for this mechanism. The energy of the product complex (**H**) is considerably higher than that of the normal binding pose (34.7 kcal/mol) and is likely to be due to the absence of water molecules to stabilize the formation of the negative charge formed on the deprotonated tyrosine side chain in the former case.

The mechanism involving proton transfer from Y169 via a bridging water molecule is shown in Figure 4d. The reaction coordinate for the proton transfer is defined differently for this pathway: The distance between one of the water hydrogen atoms and the C2 atom of substrate **1**. For this reaction pathway, the initial hydride transfer step ($\mathbf{B_W}$) has an energy barrier of 19.0 kcal/mol. The barrier to proton transfer ($\mathbf{G_W}$) is 17.2 kcal/mol and involves transfer of a proton from the water molecule to the substrate, with a simultaneous transfer of a proton from the Y169 OH group to the water molecule. Hence, as is the case for the other pathways calculated for the normal binding pose, the hydride transfer step is found to be rate limiting, and the overall barrier in this case is 19.0 kcal/mol.

In summary, from the reaction pathways shown in Figure 4, the lowest energy barrier is calculated for the normal substrate binding pose, and the rate-limiting step is the hydride transfer step. The difference in energy barrier between the pathways where the OH group of Y169 is pointing toward or away from the substrate is similar (within 1 kcal/mol). The reaction involving the flipped binding pose is considerably higher than that of the normal binding pose (by 12.8 kcal/mol). Furthermore, the calculated reaction pathways suggest that Y169 is more likely to protonate the substrate directly, rather than via a bridging water molecule.

Relaxed Potential Energy Surfaces. The minimum energy reaction pathways depicted in Figure 4 suggest that the mechanism for C═C bond reduction occurs as two distinct chemical steps, with hydride transfer occurring in the initial step. While the 2D reaction profiles provide important insight into the ordering of reaction events, refinement of these pathways, considering each step separately and calculating multiple pathways from different MD structures, will provide a more accurate description of the reaction energetics and structural representation of the stationary points. Therefore, the

DOI: 10.1021/jacs.5b08687
J. Am. Chem. Soc. 2015, 137, 14733–14742

mechanism was studied in further detail using 1D potential energy surfaces concentrating on each step separately. By only applying one reaction coordinate constraint at a time, the rest of the QM subsystem has the freedom to relax, allowing it to get closer to the true minimum energy pathway.

Hydride Transfer. The hydride transfer step was modeled using three different structural snapshots from the restrained MD simulation of the normal orientation of the substrate. Due to the conformational change observed for the flipped substrate orientation, an additional two pathways were calculated for this orientation. The calculated energy barriers to hydride abstraction are displayed in Table 2. The barriers for the normal substrate binding orientation range between 15.7 and 18.0 kcal/mol, whereas the barriers are considerably higher for the flipped orientation (22.5−33.2 kcal/mol), which indicates that where possible, the reduction of substrate **1** will occur via the normal binding pose. The lowest calculated energy barriers are slightly higher than those calculated on the 2D energy surfaces, as the transition states in the present case were optimized using the quadratic synchronous transit method. The energy barriers calculated from the portion of the simulation following the conformational change of the protein are lower than those calculated using structures that were obtained from the section prior to the conformational change.

If indeed the reaction starting from the flipped orientation is less favored, this helps to explain the high degree of stereoselectivity observed for prochiral substrates.[8−12] The reaction energies for the respective binding poses follow a similar trend: They range between 7.0 and 9.3 kcal/mol and 16.4 and 24.5 kcal/mol for the normal and flipped substrate orientations, respectively. The differences in energetics observed between poses of the same substrate orientation reflect differences in the strengths of the hydrogen-bonding interactions to the enolate intermediate.

The geometries of the lowest energy transition states to hydride abstraction for the normal and flipped docking poses are displayed in Figure 5. Selected bond lengths for the transition states are displayed in SI Table S5. The transition states for the normal orientation of the substrate occur later on the potential energy surface than those for the flipped orientation (average values of N5−H distance of 1.32 and 1.38 Å, respectively). Additionally, the distances between the carbonyl oxygen of the substrate and the two histidines (H164 and H167) are shorter for the transition states to hydride transfer for the normal orientation. Therefore, stronger hydrogen-bonding interactions between the substrate and histidines are likely to stabilize the negative charge forming on the oxygen during the hydride transfer and therefore lower the barrier for the normal binding orientation compared to the flipped one. This is likely to explain the higher barriers obtained for hydride transfer to the flipped orientation of the substrate. For the profile with the highest barrier calculated for the flipped substrate orientation (33.2 kcal/mol), the hydrogen bond to H164 is completely broken at the transition state.

The optimal angle of approach of a nucleophile to a trigonal unsaturated electrophile, referred to as the Bürgi−Dunitz angle as originally considered in nucleophilic additions to ketones,[48] can be used to explain the geometries of transition states for reactions such as the hydride transfer step modeled here. Values close to the tetrahedral angle (109.5°) are expected, as this results in the maximum amount of overlap between the HOMO of the nucleophile and the LUMO of the electrophile. Bürgi−Dunitz angles were originally obtained from crystallographic measurements and QM calculations, and significant deviations have been observed in enzyme-catalyzed reactions, such as the value of 88° observed for amide cleavage in subtilisin.[49] The Bürgi−Dunitz angles for the transition states shown in Figure 5 are 102° and 100.3° for the normal and flipped orientations of the substrate, respectively. The values for the other pathways lie between 100.1° and 107.6° (see SI Table S9), and the highest values are observed for the pathways that have the highest energy barriers. The highest value of 107.6°

Table 2. Activation Energy Barriers ($\Delta E^{\ddagger}$) and Reaction Energies (ΔE) [in kcal/mol] for Hydride Transfer from N5 of the Reduced Flavin FMNH to C3 of Substrate 1[a]

substrate orientation	profile	$\Delta E^{\ddagger}$	ΔE
normal	1	15.7	7.3
	2	16.9	7.0
	3	18.0	9.3
flipped	1[b]	32.5	22.6
	2[b]	32.9	24.5
	3[b]	33.2	19.1
	4[c]	22.5	16.4
	5[c]	25.5	20.2

[a]Calculated at the B3LYP-D3:cc-pVTZ(-f)/OPLS2005//B3LYP:6-31G(d)/OPLS2005 level. [b]Denotes starting structures that were obtained from the MD simulation prior to the observed conformation rearrangement. [c]Denotes starting structures that were obtained from the MD simulation following the observed conformation rearrangement.

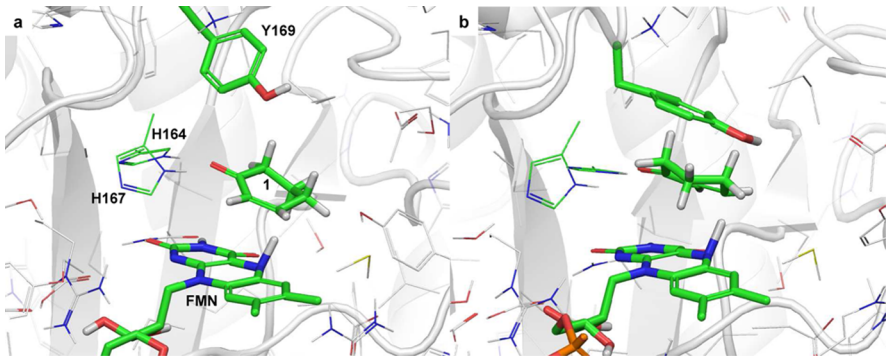

Figure 5. Transition states geometries for the lowest energy pathways calculated for hydride transfer in the (a) normal and (b) flipped orientations of **1**.

DOI: 10.1021/jacs.5b08687
J. Am. Chem. Soc. 2015, 137, 14733−14742

was calculated for the profile with the highest barrier (33.2 kcal/mol).

During the hydride transfer step, as the reaction coordinate value decreases (the distance between the N5 hydride and substrate C3), the distance between the Y169 hydroxyl proton and substrate C2 atom increases. This further supports the stepwise nature of the overall mechanism, with hydride transfer preceding proton transfer.

Proton Transfer. Using the enolate intermediates generated from modeling the hydride transfer step above, the proton transfer step was investigated. As the hydride transfer barriers for the flipped substrate orientation were unfeasibly high, only the normal substrate orientation was considered during this step. The mechanism for direct proton transfer from Y169 was found to have the lowest energy barrier in Figure 4, hence only this mechanism was considered. Three pathways were computed, and the energies of the stationary points along these pathways, calculated relative to the QM/MM minimized reactant complex, are displayed in Table 3. The highest point

Table 3. Energies of Stationary Points on 1D Potential Energy Surfaces to Direct Proton Transfer from Y169 to C2 of the Enolate Intermediate C for the Normal Orientation of Substrate 1[a]

profile	$E_{D.}$	E_E	E_F	E_G	E_H
1	22.9	16.6	9.6	15.5	9.6
2	17.5	–	5.5	10.1	−2.4
3	28.7	–	11.6	19.6	14.1

[a]Energies are given in kcal/mol relative to the energy of the reactant complex **A**. Calculated at the B3LYP-D:6-311++G(d,p)//B3LYP:6-31G(d)/OPLS2005 level of QM/MM theory.

on the potential energy surfaces calculated for the proton transfer step corresponds to rotation of the Y169 side chain, the barriers ranging between 17.5 and 28.7 kcal/mol at the B3LYP-D:6-311++G(d,p)//B3LYP:6-31G(d)/OPLS2005 level of QM/MM theory. The intermediate **F**, defined in Scheme 3, has energies ranging between 5.5 and 11.6 kcal/mol. The barrier to the proton transfer step itself has barriers ranging between 10.1 and 19.6 kcal/mol. The structure of the lowest energy transition state to proton transfer, **G**, is displayed in Figure 6. The energies of the product complex **H** range between 6.7 and 15.6 kcal/mol. The high energy of the product compared to the reactant complex can be rationalized by the formation of the tyrosine anion, which in the enzyme is expected to undergo rapid protonation. The pathway with the lowest overall barrier to reaction is pathway 1.

Overall Reaction Mechanism. The overall reaction scheme is depicted in Figure 7. The energies displayed in Figure 7 are for the normal substrate orientation and correspond to the Boltzmann-weighted average of the energies of species **A**−**H** for the three calculated pathways (calculated as outlined previously).[50] The geometries correspond to those optimized for pathway 2, as this pathway was found to be the one with the lowest overall energy barrier. The rate-limiting chemical step in the reaction is the hydride transfer step, with a barrier of 16.3 kcal/mol. The proton transfer barrier is significantly lower (10.8 kcal/mol). The highest point on the potential energy surface corresponds to the rotation of the Y169 side chain. This rotation is not required if starting from an MD structure where the proton is already pointing toward the substrate, however, as the Y169 points away from the substrate during the majority of

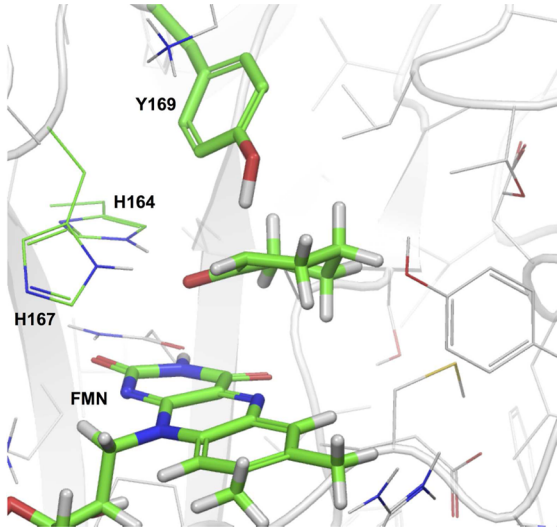

Figure 6. Transition-state geometry for the lowest energy pathway calculated for proton transfer from Y169 to C2 of intermediate **C**.

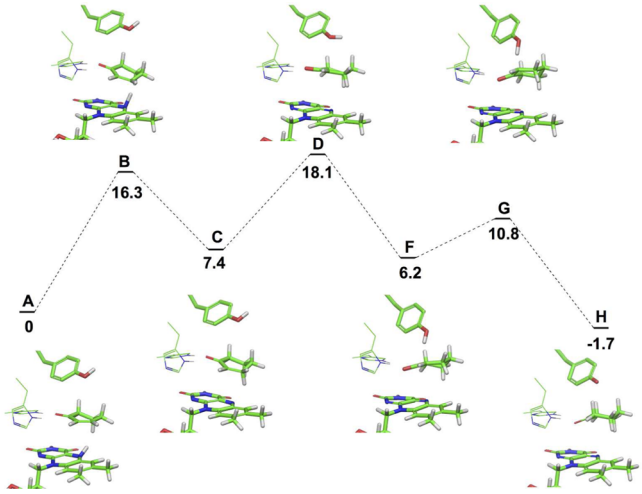

Figure 7. Overall reaction scheme for reduction of substrate **1** by YqjM. Energies are calculated relative to the reactant complex at the B3LYP-D3-cc-pVTZ//B3LYP-D/6-31G(d)/OPLS2005 level [in kcal/mol], by taking a Boltzmann-weighted average of the energies calculated for the profiles of the normal substrate binding pose.

the simulation, it may be assumed that this is a more energetically favorable orientation.

It has been proposed previously, from experimental investigations of another OYE family member, morphinone reductase, that quantum mechanical tunneling may contribute to the hydride and proton transfer processes.[13] It is not currently known whether tunneling plays a role in the reduction of substrate **1** by YqjM and to what extent. In our previous work[8] the apparent steady-state value of k_{cat} for this substrate with WT YqjM was calculated to be 2.2 s^{-1}. Neglecting contributions from tunneling and applying classical transition-state theory using the Eyring equation, this corresponds to an activation free energy of 17.0 kcal/mol. Our calculated barrier does not include a zero-point energy correction nor an entropy contribution, and therefore a direct comparison is not possible. These contributions are likely to be small (<5 kcal/mol) and of opposite sign.[51] Therefore, our overall calculated barrier of 18.1 kcal/mol seems reasonable. Such apparent good agreement is

DOI: 10.1021/jacs.5b08687
J. Am. Chem. Soc. 2015, 137, 14733−14742

perhaps fortuitous, given the limitations of the methods used here, and may be due to cancellation of errors. The aim of this study is to uncover mechanistic details, rather than to calculate high-accuracy energy barriers. Such studies have been performed for other enzymes, by employing correlated ab initio methods and performing greater conformational sampling.[52]

As mentioned in the Introduction, transition-state structures of enzyme-catalyzed reactions have the potential to aid in the design of more regio- and stereoselective mutants. For example, the active site residues that are located within closest proximity to the substrate at the transition state are likely to have the most significant effect on the course of a reaction when mutated. In order to enhance or reverse the stereoselectivity for a given prochiral α,β-unsaturated ketone, it must be energetically more favorable for the substrate to react in the normal compared to the flipped orientation or vice versa. This can be achieved by modifying the residues surrounding the substrate binding site to either stabilize or destabilize one orientation relative to the other. The residues located within 4 Å of substrate **1** over the course of the reaction are C26, Y28, A60, I69, and T70. In our directed evolution study using iterative saturation mutagenesis,[8] these residues were some of those that were found to have the largest impact on activity and selectivity of the reduction of 3-methylcyclohexen-1-one. In particular, mutating C26 to a large residue, such as tryptophan, increased the amount of *R*-selectivity for the reduction of 3-methylcyclohexen-1-one, whereas mutating the same residue to glycine reversed the selectivity in favor of formation of *S*-3-methylcyclohexan-1-one.

CONCLUSIONS AND PERSPECTIVE

Detailed mechanistic insight into the reactivity of enzymes can be useful for the design of highly selective biocatalysts. QM/MM calculations of the reaction mechanism of YqjM presented here support the proposed mechanism for OYE-catalyzed reduction of α,β-unsaturated ketones based on experimental findings. Specifically, a hydride ion is transferred from the N5 of the reduced flavin to the carbon atom β to the ketone, and a proton is supplied to the carbon atom α to the ketone from Y169. Our calculations support a mechanism by which the hydride and proton transfer steps occur as separate steps, with an enolate intermediate which has so far not been experimentally isolated. The rate-limiting chemical step for the overall reaction is hydride transfer. The hydrogen-bonding interactions between the two histidine side chains H164 and H167 are found to orient the substrate in a reactive position and also increase the polarity of the C=O bond thus facilitating the hydride transfer step. Furthermore, these interactions serve to stabilize the formation of the enolate intermediate and prevent protonation of the enolate by Y169, enabling the proton instead to transfer to the carbon atom adjacent to the carbonyl. Knowledge of the distance and angles corresponding to the low-energy transition states can be of aid to the rational design[11] or structure-guided directed evolution[8−10,12] of new active and stereoselective OYE mutants.

ASSOCIATED CONTENT

Supporting Information

The Supporting Information is available free of charge on the ACS Publications website at DOI: 10.1021/jacs.5b08687.

Further details of docking and MD simulations; absolute QM/MM energies of computed stationary points; QM coordinates of stationary points on lowest energy reaction pathway (PDF)

AUTHOR INFORMATION

Corresponding Author

*reetz@mpi-muelheim.mpg.de

Notes

The authors declare no competing financial interest.

ACKNOWLEDGMENTS

Support from the Max-Planck-Society and the LOEWE Research cluster SynChemBio is gratefully acknowledged.

REFERENCES

(1) *Modern Reduction Methods*; Andersson, P. G.; Munslow, I. J., Eds.; Wiley-VCH: Weinheim, 2008.
(2) (a) Ouellet, S. G.; Walji, A. M.; MacMillan, D. W. C. *Acc. Chem. Res.* **2007**, *40*, 1327. (b) Martin, N. J. A.; List, B. *J. Am. Chem. Soc.* **2006**, *128*, 13368.
(3) Bougioukou, D. J.; Stewart, J. D. In *Enzyme Catalysis in Organic Synthesis*; Drauz, K., Gröger, H., May, O., Eds.; Wiley-VCH Verlag GmbH & Co. KGaA: Weinheim, Germany, 2012; pp 1111−1163.
(4) Toogood, H. S.; Gardiner, J. M.; Scrutton, N. S. *ChemCatChem* **2010**, *2*, 892.
(5) Fitzpatrick, T. B.; Amrhein, N.; Macheroux, P. *J. Biol. Chem.* **2003**, *278*, 19891.
(6) Fitzpatrick, T. B.; Auweter, S.; Kitzing, K.; Clausen, T.; Amrhein, N.; MacHeroux, P. *Protein Expression Purif.* **2004**, *36*, 280.
(7) Stuermer, R.; Hauer, B.; Hall, M.; Faber, K. *Curr. Opin. Chem. Biol.* **2007**, *11*, 203.
(8) Bougioukou, D. J.; Kille, S.; Taglieber, A.; Reetz, M. T. *Adv. Synth. Catal.* **2009**, *351*, 3287.
(9) Walton, A. Z.; Sullivan, B.; Patterson-Orazem, A. C.; Stewart, J. D. *ACS Catal.* **2014**, *4*, 2307.
(10) Brenna, E.; Crotti, M.; Gatti, F. G.; Monti, D.; Parmeggiani, F.; Powell, R. W.; Santangelo, S.; Stewart, J. D. *Adv. Synth. Catal.* **2015**, *357*, 1849.
(11) Horita, S.; Kataoka, M.; Kitamura, N.; Nakagawa, T. *ChemBioChem* **2015**, *16*, 440.
(12) Forchin, M. C.; Crotti, M.; Gatti, F. G.; Parmeggiani, F.; Brenna, E.; Monti, D. *ChemBioChem* **2015**, *16*, 1571.
(13) Basran, J.; Harris, R. J.; Sutcliffe, M. J.; Scrutton, N. S. *J. Biol. Chem.* **2003**, *278*, 43973.
(14) Pang, J.; Hay, S.; Scrutton, N. S.; Sutcliffe, M. J. *J. Am. Chem. Soc.* **2008**, *130*, 7092.
(15) Kohli, R. M.; Massey, V. *J. Biol. Chem.* **1998**, *273*, 32763.
(16) Barna, T. M.; Khan, H.; Bruce, N. C.; Barsukov, I.; Scrutton, N. S.; Moody, P. C. *J. Mol. Biol.* **2001**, *310*, 433.
(17) Kitzing, K.; Fitzpatrick, T. B.; Wilken, C.; Sawa, J.; Bourenkov, G. P.; Macheroux, P.; Clausen, T. *J. Biol. Chem.* **2005**, *280*, 27904.
(18) Xu, D.; Kohli, R. M.; Massey, V. *Proc. Natl. Acad. Sci. U. S. A.* **1999**, *96*, 3556.
(19) Lonsdale, R.; Ranaghan, K. E.; Mulholland, A. J. *Chem. Commun.* **2010**, *46*, 2354.
(20) Senn, H. M.; Thiel, W. *Angew. Chem., Int. Ed.* **2009**, *48*, 1198.
(21) van der Kamp, M. W.; Mulholland, A. J. *Biochemistry* **2013**, *52*, 2708.
(22) Meier, K.; Choutko, A.; Dolenc, J.; Eichenberger, A. P.; Riniker, S.; van Gunsteren, W. F. *Angew. Chem., Int. Ed.* **2013**, *52*, 2820.
(23) Lin, H.; Truhlar, D. G. *Theor. Chem. Acc.* **2007**, *117*, 185.
(24) de Visser, S. P.; Quesne, M. G.; Martin, B.; Comba, P.; Ryde, U. *Chem. Commun.* **2014**, *50*, 262.
(25) Chateauneuf, G. M.; Brown, R. E.; Brown, B. J. *Int. J. Quantum Chem.* **2001**, *85*, 685.

DOI: 10.1021/jacs.5b08687
J. Am. Chem. Soc. 2015, 137, 14733−14742

(26) Heyes, D. J.; Sakuma, M.; de Visser, S. P.; Scrutton, N. S. *J. Biol. Chem.* **2009**, *284*, 3762.
(27) *Maestro*, version 10.0, Schrödinger, LLC: New York, 2014.
(28) Li, H.; Robertson, A.; Jensen, J. *Proteins: Struct., Funct., Genet.* **2005**, *61*, 704.
(29) *LigPrep*, version 3.2, Schrödinger, LLC: New York, 2014.
(30) (a) *Schrödinger Suite 2014-4 Induced Fit Docking protocol, Glide*, version 6.5; Schrödinger, LLC, New York, 2014. (b) *Prime*, version 3.8; Schrödinger, LLC, New York, 2014.
(31) Sherman, W.; Beard, H. S.; Farid, R. *Chem. Biol. Drug Des.* **2006**, *67*, 83.
(32) Sherman, W.; Day, T.; Jacobson, M. P.; Friesner, R. A.; Farid, R. *J. Med. Chem.* **2006**, *49*, 534.
(33) Farid, R.; Day, T.; Friesner, R. A.; Pearlstein, R. A. *Bioorg. Med. Chem.* **2006**, *14*, 3160.
(34) *Desmond Molecular Dynamics System*, version 4.0, D. E. Shaw Research: New York, 2014. (b) *Maestro-Desmond Interoperability Tools*, version 4.0, Schrödinger, LLC, New York, 2014.
(35) Shivakumar, D.; Williams, J.; Wu, Y.; Damm, W.; Shelley, J.; Sherman, W. *J. Chem. Theory Comput.* **2010**, *6*, 1509.
(36) Guo, Z.; Mohanty, U.; Noehre, J.; Sawyer, T. K.; Sherman, W.; Krilov, G. *Chem. Biol. Drug Des.* **2010**, *75*, 348.
(37) Bowers, K. J.; Chow, E.; Xu, H.; Dror, R. O.; Eastwood, M. P.; Gregersen, B. A.; Klepeis, J. L.; Kolossvary, I.; Moraes, M. A.; Sacerdoti, F. D.; Salmon, J. K.; Shan, Y.; Shaw, D. E. In Proceedings of the 2006 ACM/IEEE conference on Supercomputing, Tampa, FL, November 11−17, 2006; ACM: New York, 2006.
(38) Banks, J. L.; Beard, H. S.; Cao, Y.; Cho, A. E.; Damm, W.; Farid, R.; Felts, A. K.; Halgren, T. A.; Mainz, D. T.; Maple, J. R.; Murphy, R.; Philipp, D. M.; Repasky, M. P.; Zhang, L. Y.; Berne, B. J.; Friesner, R. A.; Gallicchio, E.; Levy, R. M. *J. Comput. Chem.* **2005**, *26*, 1752.
(39) Jorgensen, W. L.; Chandrasekhar, J.; Madura, J. D.; Impey, R. W.; Klein, M. L. *J. Chem. Phys.* **1983**, *79*, 926.
(40) *Impact*, version 6.5; Schrödinger, LLC: New York, 2014.
(41) *QSite*, version 6.5; Schrödinger, LLC: New York, 2014.
(42) Murphy, R. B.; Philipp, D. M.; Friesner, R. A. *J. Comput. Chem.* **2000**, *21*, 1442.
(43) Philipp, D. M.; Friesner, R. A. *J. Comput. Chem.* **1999**, *20*, 1468.
(44) Lonsdale, R.; Harvey, J. N.; Mulholland, A. J. *J. Chem. Theory Comput.* **2012**, *8*, 4637.
(45) Grimme, S.; Antony, J.; Ehrlich, S.; Krieg, H. *J. Chem. Phys.* **2010**, *132*, 154104.
(46) *Jaguar*, version 8.6, Schrödinger, LLC: New York, 2014.
(47) Bochevarov, A. D.; Harder, E.; Hughes, T. F.; Greenwood, J. R.; Braden, D. A.; Philipp, D. M.; Rinaldo, D.; Halls, M. D.; Zhang, J.; Friesner, R. A. *Int. J. Quantum Chem.* **2013**, *113*, 2110.
(48) Buergi, H. B.; Dunitz, J. D. *Acc. Chem. Res.* **1983**, *16*, 153.
(49) Radisky, E. S.; Koshland, D. E. *Proc. Natl. Acad. Sci. U. S. A.* **2002**, *99*, 10316.
(50) Lonsdale, R.; Harvey, J. N.; Mulholland, A. J. *J. Phys. Chem. B* **2010**, *114*, 1156.
(51) Villa, J.; Strajbl, M.; Glennon, T. M.; Sham, Y. Y.; Chu, Z. T.; Warshel, a. *Proc. Natl. Acad. Sci. U. S. A.* **2000**, *97*, 11899.
(52) Claeyssens, F.; Harvey, J. N.; Manby, J. N.; Mata, R. A.; Mulholland, A. J.; Ranaghan, K. E.; Schütz, M.; Thiel, S.; Thiel, W.; Werner, H.-J. *Angew. Chem., Int. Ed.* **2006**, *45*, 6856.

■ NOTE ADDED AFTER ASAP PUBLICATION

Reference 2b was added on November 25, 2015.

DOI: 10.1021/jacs.5b08687
J. Am. Chem. Soc. 2015, 137, 14733−14742